Novelty detection using ensembles with regularized disagreement

Alexandru Țifrea [1] **Eric Stavarache** [1] **Fanny Yang** [1]

Abstract

Novelty detection methods should flag samples that are not similar to the training data (ID), for example when new classes emerge over time (OOD). Even though current OOD detection algorithms can successfully distinguish completely different data sets, they fail to reliably identify samples from novel classes. We develop a new ensemble-based procedure that promotes model diversity and exploits regularization to limit disagreement to only OOD samples, using a batch containing an unknown mixture of ID and OOD data. We show that our procedure significantly outperforms state-of-the-art methods, including those that have access, during training, to data that is known to be OOD. We run extensive comparisons of our approach on a variety of novel-class detection scenarios, on standard image data sets such as SVHN/CIFAR-10/CIFAR-100 as well as on new disease detection on medical image data sets.[1]

1. Introduction

Modern machine learning (ML) systems are gaining popularity in many real-world applications, from aiding medical diagnosis (Beede et al., 2020) to making recommendations for the justice system (Angwin et al., 2016). Despite achieving great test set performance, many approaches have trouble dealing with out-of-distribution (OOD) data, i.e. test inputs that are unlike the data seen during training. For example, ML models often make incorrect predictions with high confidence when new unseen classes emerge over time (e.g. undiscovered bacteria (Ren et al., 2019), new diseases (Katsamenis et al., 2020)), or when data suffers from distribution shift (e.g. corruptions (Lu et al., 2019), environmental changes (Kumar et al., 2020)). If the OOD data consists of novel classes, then we must identify the OOD samples and bring them to the attention of human experts. This scenario is the focus of this paper and we use the terms OOD and novelty detection interchangeably.

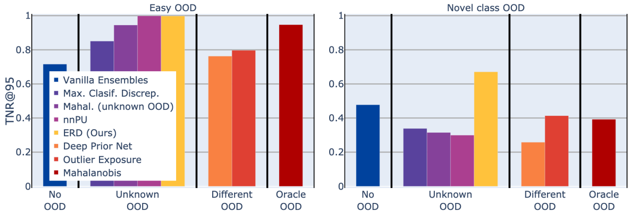

Figure 1. Comparison of OOD detection methods ordered by the amount of information about the OOD distribution that they require. **Left:** On the easy settings usually reported in the literature, many methods achieve near-perfect detection. **Right:** On novel-class settings where ID and OOD data are difficult to distinguish, most baselines reach a much lower TNR@95 compared to our method.

Novelty detection aims to identify test samples that have a low probability under the marginal ID distribution P_X, i.e. x should be flagged as OOD if $P_X(x) \leq \alpha$ for some small constant α. If we could learn a model that estimates precisely the level sets of P_X, we would have perfect OOD detection. Unfortunately, when the input space is high-dimensional and we only have access to limited data, this problem is intractable. In reality, however, we only need to detect outliers that actually appear in a test set, which makes the problem more amenable to statistical methods.

Apart from a labeled ID training set, state-of-the-art (SOTA) OOD detection methods often use some OOD data for training or calibration. We separate existing approaches into four different levels of access to OOD data: 1) *no OOD* data (Lakshminarayanan et al., 2017; Sastry & Oore, 2019); 2) an unlabeled set with an unknown mixture of ID and OOD data where OOD samples are not marked (*Unknown OOD*) (Scott & Blanchard, 2008; du Plessis et al., 2014; Liu et al., 2018; Yu & Aizawa, 2019); 3) known OOD data, but from a different distribution than the test OOD (*Different OOD*) (Hendrycks et al., 2019; Malinin & Gales, 2018); or 4) known OOD data from the same distribution as test OOD (*Oracle OOD*) (Lee et al., 2018; Liang et al., 2018).

Notably, prior work on OOD detection reports remarkably good detection performance: when 95% of the true OOD samples are correctly identified (i.e. the true positive rate is 95%), the ratio of ID samples correctly identified as ID

[*] Equal contribution [1] Department of Computer Science, ETH Zurich, Switzerland. Correspondence to: Alexandru Țifrea <tifreaa@inf.ethz.ch>.

Presented at the ICML 2021 Workshop on Uncertainty and Robustness in Deep Learning., Copyright 2021 by the author(s).

[1] Our code is available at https://github.com/ericpts/reto.

Algorithm 1 Fine-tuning the ERD ensemble

```
Input: Train set $S$, Validation set $V$, Unlabeled set $U$, Weights $W$ pretrained on $S$, Ensemble size $K$
Output: ERD ensemble $\{f_{y_i}\}_{i=1}^K$
Sample $K$ different labels $\{y_1, ..., y_K\}$ from $\mathcal{Y}$
for all $c \in \{y_1, ..., y_K\}$ do
    $f_c \leftarrow$ Initialize$(W)$
    $(U, c) \leftarrow \{(x, c) : x \in U\}$
    $f_c \leftarrow$ FinetuneWithEarlyStopping $(f_c, S \cup (U, c); V)$
end for
return $\{f_{y_i}\}_{i=1}^K$
```

Algorithm 2 OOD detection with ERD

```
Input: Ensemble $\{f_{y_i}\}_{i=1}^K$, Test set $T$, Threshold $t_0$, Disagreement metric $\rho$
Output: $O$, i.e. the OOD elements of $T$
$O \leftarrow \emptyset$
for all $x \in U$ do
    if $(\text{Avg} \circ \rho)(f_{y_1}, ..., f_{y_K})(x) > t_0$ then
        $O \leftarrow O \cup \{x\}$
    end if
end for
return $O$
```

(i.e. the true negative rate) is often larger than 80% (this metric is known as the TNR@95). However, these numbers are largely obtained when the in-distribution (ID) and the OOD data sets are vastly different (e.g. SVHN vs CIFAR10), while in real-world applications it is unlikely that the novel data is so easy to distinguish from ID samples (e.g. chest X-rays of a new disease may look quite similar to another pathology). When evaluating state-of-the-art (SOTA) methods on novel-class settings on standard image data sets (e.g. SVHN, CIFAR10), the TNR@95 for the best baseline drops below 40% (see Figure 1 Right).

In this work, we adopt the *Unknown OOD* setting and introduce a principled method to obtain diverse ensembles by leveraging the unlabeled set and using early stopping regularization. We call our method **Ensembles with Regularized Disagreement (ERD)** and motivate it using a theoretical result on the dynamics of gradient descent training under label noise. Furthermore, we design a disagreement-based score for ensembles and argue that it successfully exploits model diversity, and thus helps ERD achieve significant improvements compared to SOTA approaches. Our method improves the state-of-the-art for novel-class detection, surpassing even approaches that assume oracle knowledge of OOD samples, as illustrated in Figure 1.

2. Problem setting

In this section we motivate the *Unknown OOD* setting that we adopt for our method and stress its practical relevance.

Problem statement. We consider a labeled data set $S = \{(x_i, y_i)\}_{i=1}^n \sim P$, where $x_i \in \mathcal{X}$ are the covariates and $y_i \in \mathcal{Y}$ are discrete labels. We assume that the labels are obtained as a deterministic function of the covariates, which we denote $y^* : \mathcal{X} \to \mathcal{Y}$. In this paper we focus on detecting samples from novel classes, unseen at training time. We define $\mathcal{X}_{ID} := \{x : P_X(x) > \alpha\}$ as ID points and $\mathcal{X}_{OOD} = \{x : P_X(x) \leq \alpha\}$ as the set of OOD points, where P_X is the marginal ID distribution.

The *Unknown OOD* settings has been proposed in prior work on OOD detection (Scott & Blanchard, 2008; Liu et al., 2018; Yu & Aizawa, 2019) and assumes that, apart from the ID training data with class labels, we also have access to a batch of unlabeled data U drawn from the same distribution P_{test} as the test data. This distribution consists of a mixture of ID and OOD data, with OOD proportion $\pi \in [0, 1]$, that is $P_{\text{test}}[x \in \mathcal{X}_{OOD}] = \pi$. The goal is to use the set U to learn to distinguish between ID and OOD data drawn from P_{test}, without explicit knowledge of π nor which samples in U are OOD.

The *Unknown OOD* setting is relevant for many practical applications that would benefit from more effective novel-class detection. Consider, for instance, a medical center that uses an automated system for real-time diagnosis. In addition, the hospital may wish to run a novelty detection algorithm offline every week to check for possible new pathologies. A procedure based on the unknown OOD setting can use all the X-rays from the week as an unlabeled set U. If U contains X-rays exhibiting a new disease, the algorithm can be used to flag such novel classes both in the already collected unlabeled set and for future patients suffering from the same new disease. Furthermore, the flagged samples can be examined and labeled by experts.

3. Proposed method

In this section we introduce our proposed algorithm, ERD, and provide a principled justification for the key ingredients that lead to the improved performance of our method.

3.1. The complete ERD procedure

Recall that we have access to both a labeled training set S and an unlabeled set U that contains both ID and unknown OOD samples. Moreover, we initialize the models of the ensemble using weights pretrained on S.

In Algorithm 1 we show how to obtain an ERD ensemble. We begin by assigning an arbitrary label $c \in \mathcal{Y}$, to all the unlabeled samples in U, resulting in the c-labeled set $(U, c) := \{(x, c) : x \in U\}$. We then fine-tune a classifier f_c on the union $S \cup (U, c)$ of the correctly-labeled training set S and the unlabeled set (U, c). We perform early stopping by picking a model at an intermediate epoch, before the accuracy on a holdout ID validation set V starts to decrease. We repeat this procedure to create an ensemble of several classifiers f_c, for different choices of $c \in \mathcal{Y}$. Finally, during test time in Algorithm 2, we use this ensemble to flag as OOD all the points for which an aggregate disagreement

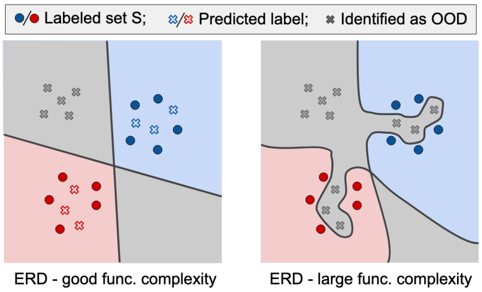

Figure 2. Restricting model complexity is necessary to prevent from flagging the whole U as OOD. **Left:** Linear classifiers disagree on points in U_{OOD}, but agree to predict the correct label on samples from U_{ID}. **Right:** The models are too complex so they fit the arbitrary label on the entire U.

measure surpasses a threshold value t_0, as we elaborate later in this section.

Role of regularization. Recall that, in our approach, each member of the ensemble tries to fit a different label c to the entire unlabeled set U in addition to the correct labels of the ID training set S. We train the models to fit $S \cup (U, c)$, where we use the notation $(U, c) = (U_{\mathrm{ID}}, c) \cup (U_{\mathrm{OOD}}, c) = \{(x, c) : x \in U_{\mathrm{ID}}\} \cup \{(x, c) : x \in U_{\mathrm{OOD}}\}$. Moreover, we can partition the set (U_{ID}, c) into the subset of samples whose ground truth label differs from c and are thus incorrectly labeled with c, and the subset whose correct label is indeed c:

$$(U_{\mathrm{ID}}^{\neg c}, c) := \{(x, c) : x \in U_{\mathrm{ID}} \text{ with } y^*(x) \neq c\}$$
$$(U_{\mathrm{ID}}^{c}, c) := \{(x, c) : x \in U_{\mathrm{ID}} \text{ with } y^*(x) = c\}$$

We now explain why and how we can regularize the model complexity such that the classifier fits S and all of (U, c), except for $(U_{\mathrm{ID}}^{\neg c}, c)$. The *key intuition* why regularization helps is that it is more difficult to fit the labels c on $(U_{\mathrm{ID}}^{\neg c}, c)$ than on (U_{OOD}, c), since $(U_{\mathrm{ID}}^{\neg c}, c)$ lies closer in covariate space to points in the correctly labeled training set S. Hence, we can exactly fit (U_{OOD}, c) but not the entire (U_{ID}, c) if we adequately limit the function complexity (e.g. by choosing a small model class, or through regularization), as illustrated in Figure 2 Left. Moreover, since regularized predictors are smooth, it follows that the model generalizes well on ID data and also predicts the label c on holdout OOD samples similar to the ones in the U_{OOD}. On the other hand, if the models are too complex (e.g. deep neural networks (Zhang et al., 2016)), then they can even fit the wrong labels on (U_{ID}, c) (see Figure 2 Right), causing the models in the ensemble to disagree on the entire unlabeled set U.

We use early stopping regularization, motivated by recent empirical and theoretical works that have found that early stopped neural networks are less vulnerable to label noise in the training data(Yilmaz & Heckel, 2019; Li et al., 2020). We argue rigorously in Section B that there exists an optimal stopping time for gradient descent at which all points in (U, c) are fit, except for the wrongly labeled samples in (U_{ID}, c). To find the best stopping time in practice, we use a validation set of labeled ID points to select an intermediate checkpoint before convergence.

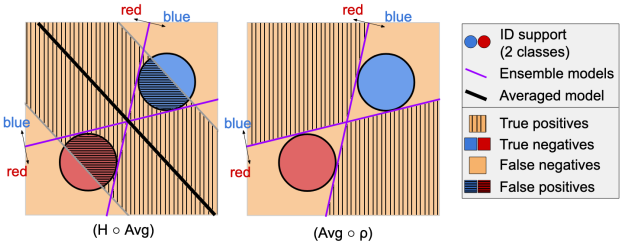

Figure 3. Cartoon illustration showing a diverse ensemble (solid purple) of linear binary classifiers. We compare OOD detection performance for two aggregation scores: (H $\circ$ Avg) (**Left**) and (Avg $\circ$ ρ) with $\rho(f_1(x), f_2(x)) = \mathbb{1}_{\mathrm{sgn}(f_1(x)) \neq \mathrm{sgn}(f_2(x))}$ (**Right**). The two metrics achieve similar TPRs, but using (H $\circ$ Avg) instead of our score, (Avg $\circ$ ρ), leads to more false positives, since the former can only flag as OOD a band around the averaged model (solid black) and cannot take advantage of the ensemble's diversity.

Ensemble disagreement score. We now motivate a novel ensemble aggregation technique tailored to exploit ensemble diversity that we use to detect OOD samples with ERD. Note that we can cast the OOD detection problem as a hypothesis test with null hypothesis $H_0 : x \in \mathcal{X}_{ID}$. Our procedure tests the null hypothesis by using an ensemble-based score: The null hypothesis is *rejected* and we report x as OOD (*positive*) if the score is larger than a threshold t_0 (see Algorithm 2).

Previous works (Lakshminarayanan et al., 2017; Ovadia et al., 2019) first average the softmax predictions of the models in the ensemble $\bar{f}(x) := \frac{1}{K}\sum_{i=1}^{K} f_i(x) \in [0, 1]^{|\mathcal{Y}|}$ and then use the entropy of $\bar{f}(x)$ as a metric, i.e. $(\mathrm{H} \circ \mathrm{Avg})(f_1(x), ..., f_K(x)) := -\sum_{i=1}^{|\mathcal{Y}|}(\bar{f}(x))_i \log(\bar{f}(x))_i$ where $(\bar{f}(x))_i$ denotes the i^{th} element of $\bar{f}(x)$. We argue that averaging model outputs first, discards information about the diversity of the ensemble. Instead, we propose the average pairwise *disagreement* between the outputs of K models in an ensemble:

$$(\mathrm{Avg} \circ \rho)(\{f_i(x)\}_{i=1}^{K}) := \frac{2}{K(K-1)} \sum_{i \neq j} \rho\left(f_i(x), f_j(x)\right),$$

where ρ is a measure of disagreement between the softmax outputs of two predictors, for example the total variation distance $\rho_{\mathrm{TV}}(f_i(x), f_j(x)) = \frac{1}{2}\|f_i(x) - f_j(x)\|_1$ used in our experiments.

In the sketch in Figure 3 we show that the score we propose, (Avg $\circ$ ρ), achieves a higher TNR compared to (H $\circ$ Avg), for a fixed TPR – a common way of evaluating statistical tests. Notice that the detection region for (H $\circ$ Avg) is always limited to a band around the average model. In order for the (H $\circ$ Avg) to have large TPR, this band needs to

Table 1. AUROC and TNR@95 for different OOD detection scenarios (the numbers in squared brackets indicate the ID or OOD classes). We highlight the **best ERD** variant and the ***best baseline*** among prior work. The asterisk marks methods proposed in this paper. nnPU (†) assumes oracle knowledge of the OOD ratio in the unlabeled set.

		Other settings					Unknown OOD				
ID data	OOD data	Vanilla Ensembles	Gram	DPN	OE	Mahal.	nnPU†	MCD	Mahal-U	Bin. Classif. *	ERD *
		AUROC ↑ / TNR@95 ↑									
SVHN	CIFAR10	0.97 / 0.88	0.97 / 0.86	***1.00*** / ***1.00***	***1.00*** / ***1.00***	0.99 / 0.98	***1.00*** / ***1.00***	0.97 / 0.85	0.99 / 0.95	1.00 / 1.00	**1.00** / **0.99**
CIFAR10	SVHN	0.92 / 0.78	***1.00*** / 0.98	0.95 / 0.85	0.97 / 0.89	0.99 / 0.96	***1.00*** / ***1.00***	***1.00*** / 0.98	0.99 / 0.96	1.00 / 1.00	**1.00** / **1.00**
CIFAR100	SVHN	0.84 / 0.48	0.99 / 0.97	0.77 / 0.44	0.82 / 0.50	0.98 / 0.90	***1.00*** / ***1.00***	0.97 / 0.73	0.98 / 0.92	1.00 / 1.00	**1.00** / **1.00**
FMNIST [0,2,3,7,8]	FMNIST [1,4,5,6,9]	0.64 / 0.07	– / –	0.77 / 0.15	0.66 / 0.12	0.77 / 0.20	***0.95*** / ***0.71***	0.78 / 0.30	0.82 / 0.39	0.95 / 0.66	**0.94** / **0.67**
SVHN [0:4]	SVHN [5:9]	0.92 / 0.69	0.81 / 0.31	0.87 / 0.19	0.85 / 0.52	0.92 / 0.71	***0.96*** / ***0.73***	0.91 / 0.51	0.91 / 0.63	0.81 / 0.40	**0.95** / **0.74**
CIFAR10 [0:4]	CIFAR10 [5:9]	0.80 / 0.39	0.67 / 0.15	***0.82*** / 0.32	***0.82*** / ***0.41***	0.79 / 0.27	0.61 / 0.11	0.69 / 0.25	0.64 / 0.13	0.85 / 0.43	**0.93** / **0.70**
CIFAR100 [0:49]	CIFAR100 [50:99]	***0.78*** / ***0.35***	0.71 / 0.16	0.70 / 0.26	0.74 / 0.31	0.72 / 0.20	0.53 / 0.06	0.70 / 0.26	0.72 / 0.19	0.66 / 0.13	**0.82** / **0.44**
Average		0.84 / 0.52	0.86 / 0.57	0.84 / 0.46	0.84 / 0.54	***0.88*** / 0.60	0.86 / ***0.66***	0.86 / 0.55	0.86 / 0.60	0.89 / 0.66	**0.95** / **0.79**

be wide, leading to many false positives. This example demonstrates how averaging softmax outputs relinquishes the benefits of a diverse ensemble that our disagreement score can exploit. Appendix C provides further quantitative evidence to support the intuition presented in Figure 3.

4. Experimental results

ID vs OOD settings. We report results on two broad types of OOD detection scenarios: **(1) Easy OOD data:** ID and OOD samples come from strikingly different data sets (e.g. CIFAR10 vs SVHN). These are the settings usually considered in the literature and on which most baselines perform well; and **(2) Hard OOD data:** The OOD data consists of "novel" classes that resemble the ID samples: e.g. the first 5 classes of CIFAR10 are ID, the last 5 classes are OOD. The similarities between the ID and the OOD classes make these settings significantly more challenging. We defer the details regarding the data sets to Appendix E.

Apart from using these canonical data sets, we also evaluate our method on more realistic data, namely a recently proposed OOD detection benchmark for medical imaging (Cao et al., 2020), described in detail in Appendix G.

Baselines. We compare ERD against previous methods that are applicable to the unknown OOD setting and also include well-known baselines that require different kinds of access to OOD data for training, as indicated in Table 3. In addition, we propose a novel simple approach that uses an unlabeled set: an early stopped binary classifier (*Bin. Classif.*) trained to distinguish between S and U. We include a detailed description of all the baselines together with precise hyperparameter choices in Appendix D.

Our method – ERD. For our method we train ensembles of 5 MLP models for FashionMNIST and ResNet20 (He et al., 2016) models for the other settings. The networks are initialized with weights pretrained on the ID training set. For each model in the ensemble we perform post-hoc early stopping: we train for 10 epochs and select the iteration with the lowest validation loss. In the appendix we also present results for a variant of ERD trained from random initializations.

Evaluation metrics. We use two standard metrics common in the OOD detection literature: the area under the ROC curve (AUROC; larger values are better) and the TNR at a TPR of 95% (TNR@95; larger values are better).

4.1. Main results

Table 1 summarizes the main empirical results. On the easy scenarios (top part of the table) most methods achieve near-perfect OOD detection with AUROC close to 1. However, on the novelty detection scenarios (bottom part), ERD has a clear edge over the other approaches and improves the average TNR@95 by 20% relative to the best baseline. Furthermore, on the novel-class setting on CIFAR10, the TPR@95 gains of our method compared to the best prior work go as high as 70%. A similar trend can be observed for AUROC as well.

On the medical OOD detection benchmark our method improves the average AUROC from 0.85 to 0.91, compared to the best performing baseline. Appendix G contains more detailed results for the medical settings.

5. Conclusions

Reliable OOD detection is essential in order to deploy classification systems in the real world. We propose a procedure that results in an ensemble with selective disagreement only on OOD data, by successfully leveraging unlabeled data to fine-tune the models in the ensemble. It outperforms state-of-the-art methods that also have access to a mixture of ID and unknown OOD samples, and even surpasses approaches that use known OOD data for training.

References

Angwin, J., Larson, J., Mattu, S., and Kirchner, L. Machine bias: There's software used across the country to predict future criminals. and it's biased against blacks. 2016.

Barbu, A., Mayo, D., Alverio, J., Luo, W., Wang, C., Gutfreund, D., Tenenbaum, J., and Katz, B. ObjectNet: A large-scale bias-controlled dataset for pushing the limits of object recognition models. In *Advances in Neural Information Processing Systems 32*, pp. 9453–9463. 2019.

Beede, E., Baylor, E., Hersch, F., Iurchenko, A., Wilcox, L., Ruamviboonsuk, P., and Vardoulakis, L. M. A human-centered evaluation of a deep learning system deployed in clinics for the detection of diabetic retinopathy. In *Proceedings of the CHI Conference on Human Factors in Computing Systems*, pp. 1–12, 2020.

Ben-David, S., Blitzer, J., Crammer, K., and Pereira, F. Analysis of representations for domain adaptation. In *Advances in Neural Information Processing Systems 19*, pp. 137–144, 2007.

Blundell, C., Cornebise, J., Kavukcuoglu, K., and Wierstra, D. Weight uncertainty in neural networks. In *Proceedings of the 32th International Conference on Machine Learning*, 2015.

Cao, T., Huang, C.-W., Hui, D. Y.-T., and Cohen, J. P. A benchmark of medical out of distribution detection. *arXiv preprint arXiv:2007.04250*, 2020.

Chen, Y., Wei, C., Kumar, A., and Ma, T. Self-training avoids using spurious features under domain shift. *arXiv preprint arXiv:2006.10032*, 2020.

Choi, H., Jang, E., and Alemi, A. A. WAIC, but why? generative ensembles for robust anomaly detection. *arXiv preprint arXiv:1810.01392*, 2018.

Deng, J., Dong, W., Socher, R., Li, L.-J., Li, K., and Fei-Fei, L. ImageNet: A large-scale hierarchical image database. In *Proceedings of the IEEE Conference on Computer Vision and Pattern Recognition (CVPR)*, 2009.

du Plessis, M. C., Niu, G., and Sugiyama, M. Analysis of learning from positive and unlabeled data. In *Advances in Neural Information Processing Systems 27*, 2014.

Fu, Y., Hospedales, T. M., Xiang, T., and Gong, S. Transductive multi-view zero-shot learning. *IEEE Transactions on Pattern Analysis and Machine Intelligence*, 37: 2332–2345, 2015.

Gal, Y. and Ghahramani, Z. Dropout as a Bayesian approximation: Representing model uncertainty in deep learning. volume 48 of *Proceedings of Machine Learning Research*, pp. 1050–1059, 2016.

Ganin, Y., Ustinova, E., Ajakan, H., Germain, P., Larochelle, H., Laviolette, F., March, M., and Lempitsky, V. Domain-adversarial training of neural networks. *Journal of Machine Learning Research*, pp. 1–35, 2016.

Geifman, Y. and El-Yaniv, R. Selective classification for deep neural networks. In *Advances in Neural Information Processing Systems 30*, pp. 4878–4887. 2017.

Graves, A. Practical variational inference for neural networks. In *Advances in Neural Information Processing Systems 24*, pp. 2348–2356. 2011.

He, K., Zhang, X., Ren, S., and Sun, J. Deep residual learning for image recognition. In *Proceedings of the IEEE Conference on Computer Vision and Pattern Recognition (CVPR)*, 2016.

Hein, M., Andriushchenko, M., and Bitterwolf, J. Why ReLU networks yield high-confidence predictions far away from the training data and how to mitigate the problem. In *Proceedings of the IEEE Conference on Computer Vision and Pattern Recognition (CVPR)*, 2019.

Hendrycks, D. and Dietterich, T. Benchmarking neural network robustness to common corruptions and perturbations. In *Proceedings of the International Conference on Learning Representations*, 2019.

Hendrycks, D., Mazeika, M., and Dietterich, T. Deep anomaly detection with outlier exposure. In *Proceedings of the International Conference on Learning Representations*, 2019.

Katsamenis, I., Protopapadakis, E., Voulodimos, A., Doulamis, A., and Doulamis, N. Transfer learning for covid-19 pneumonia detection and classification in chest x-ray images. *medRxiv*, 2020.

Kirichenko, P., Izmailov, P., and Wilson, A. G. Why normalizing flows fail to detect out-of-distribution data. In *Advances in Neural Information Processing Systems 33*, pp. 20578–20589, 2020.

Kiryo, R., Niu, G., du Plessis, M. C., and Sugiyama, M. Positive-unlabeled learning with non-negative risk estimator. In *Advances in Neural Information Processing Systems 30*, 2017.

Krizhevsky, A. Learning multiple layers of features from tiny images. Technical report, 2009.

Kumar, A., Ma, T., and Liang, P. Understanding self-training for gradual domain adaptation. *arXiv preprint arXiv:2002.11361*, 2020.

Lakshminarayanan, B., Pritzel, A., and Blundell, C. Simple and scalable predictive uncertainty estimation using deep ensembles. In Guyon, I., Luxburg, U. V., Bengio, S., Wallach, H., Fergus, R., Vishwanathan, S., and Garnett, R. (eds.), *Advances in Neural Information Processing Systems 30*, pp. 6402–6413. Curran Associates, Inc., 2017.

Lecun, Y., Bottou, L., Bengio, Y., and Haffner, P. Gradient-based learning applied to document recognition. In *Proceedings of the IEEE*, pp. 2278–2324, 1998.

Lee, K., Lee, K., Lee, H., and Shin, J. A simple unified framework for detecting out-of-distribution samples and adversarial attacks. In *Advances in Neural Information Processing Systems 31*, pp. 7167–7177. 2018.

Li, M., Soltanolkotabi, M., and Oymak, S. Gradient descent with early stopping is provably robust to label noise for overparameterized neural networks. Proceedings of Machine Learning Research, pp. 4313–4324, 2020.

Liang, S., Li, Y., and Srikant, R. Enhancing the reliability of out-of-distribution image detection in neural networks. In *Proceedings of the International Conference on Learning Representations*, 2018.

Liu, S., Garrepalli, R., Dietterich, T., Fern, A., and Hendrycks, D. Open category detection with PAC guarantees. pp. 3169–3178, 2018.

Lu, A. X., Lu, A. X., Schormann, W., Andrews, D. W., and Moses, A. M. The cells out of sample (COOS) dataset and benchmarks for measuring out-of-sample generalization of image classifiers. *arXiv preprint arXiv:1906.07282*, 2019.

Malinin, A. and Gales, M. Predictive uncertainty estimation via prior networks. In *Advances in Neural Information Processing Systems 32*, pp. 7047–7058, 2018.

Nalisnick, E., Matsukawa, A., Teh, Y. W., Gorur, D., and Lakshminarayanan, B. Do deep generative models know what they don't know? In *Proceedings of the International Conference on Learning Representations*, 2019.

Neal, R. M. *Bayesian Learning for Neural Networks*. Springer-Verlag, 1996.

Netzer, Y., Wang, T., Coates, A., Bissacco, A., Wu, B., and Ng, A. Y. Reading digits in natural images with unsupervised feature learning. In *NIPS Workshop on Deep Learning and Unsupervised Feature Learning 2011*, 2011.

Ovadia, Y., Fertig, E., Ren, J., Nado, Z., Sculley, D., Nowozin, S., Dillon, J., Lakshminarayanan, B., and Snoek, J. Can you trust your model's uncertainty? Evaluating predictive uncertainty under dataset shift. In *Advances in Neural Information Processing Systems 32*, pp. 13991–14002. 2019.

Recht, B., Roelofs, R., Schmidt, L., and Shankar, V. Do cifar-10 classifiers generalize to cifar-10? *arXiv preprint arXiv:1806.00451*, 2018.

Recht, B., Roelofs, R., Schmidt, L., and Shankar, V. Do ImageNet classifiers generalize to ImageNet? *arXiv preprint arXiv:1902.10811*, 2019.

Ren, J., Liu, P. J., Fertig, E., Snoek, J., Poplin, R., Depristo, M., Dillon, J., and Lakshminarayanan, B. Likelihood ratios for out-of-distribution detection. In *Advances in Neural Information Processing Systems 32*, pp. 14707–14718. 2019.

Sastry, C. S. and Oore, S. Detecting out-of-distribution examples with in-distribution examples and gram matrices. *arXiv preprint arXiv:1912.12510*, 2019.

Scott, C. and Blanchard, G. Transductive anomaly detection. Technical report, 2008.

Shimodaira, H. Improving predictive inference under covariate shift by weighting the log-likelihood function. *Journal of Statistical Planning and Inference*, 90:227–244, 2000.

Torralba, A., Fergus, R., and Freeman, W. T. 80 million tiny images: A large data set for nonparametric object and scene recognition. *IEEE Transactions on Pattern Analysis and Machine Intelligence*, pp. 1958–1970, 2008.

Vapnik, V. N. *Statistical Learning Theory*. Wiley-Interscience, 1998.

Wan, Z., Chen, D., Li, Y., Yan, X., Zhang, J., Yu, Y., and Liao, J. Transductive zero-shot learning with visual structure constraint. In *Advances in Neural Information Processing Systems 32*, pp. 9972–9982, 2019.

Xiao, H., Rasul, K., and Vollgraf, R. Fashion-MNIST: A novel image dataset for benchmarking machine learning algorithms, 2017.

Yilmaz, F. F. and Heckel, R. Image recognition from raw labels collected without annotators. *arXiv preprint arXiv:1910.09055*, 2019.

Yu, Q. and Aizawa, K. Unsupervised out-of-distribution detection by maximum classifier discrepancy. In *Proceedings of the IEEE/CVF International Conference on Computer Vision (ICCV)*, 2019.

Zagoruyko, S. and Komodakis, N. Wide residual networks. In *Proceedings of the British Machine Vision Conference (BMVC)*, 2016.

Zhang, C., Bengio, S., Hardt, M., Recht, B., and Vinyals, O. Understanding deep learning requires rethinking generalization. *arXiv preprint arXiv:1611.03530*, 2016.

A. Related work

A.1. Limitations of related OOD detection methods

We now discuss some shortcomings of existing OOD detection approaches closely related to ours and indicate how our method attempts to address them. Firstly, vanilla ensembles use only the stochasticity of the training process and the random initialization to obtain diverse models, but this often leads to similar classifiers, that predict the same incorrect label on OOD data (Hein et al., 2019). Secondly, in the absence of proper regularization, optimizing the MCD objective leads to models that agree to a similar extent on both ID and OOD data so that one cannot distinguish them from one another (as indicated by low AUROC scores). Furthermore, nnPU does not exploit all the signal in the training set and discards the labels of the ID data.

ERD successfully diversifies an ensemble on OOD data by using the unlabeled set and without requiring additional information about the test distribution (e.g. unlike nnPU which requires the true OOD ratio). We identify the key reasons behind the good performance of our approach to be as follows: 1) utilizing the labels of the ID training data and the complexity of deep neural networks to diversify model outputs on OOD data; 2) choosing an appropriate disagreement score that draws on ensemble diversity; 3) employing early stopping regularization to prevent diversity on ID inputs.

A.2. Related problems

Predictive uncertainty and Bayesian methods. One of the important appeals of the Bayesian framework is that it directly provides uncertainty estimates together with the predictions. Bayesian methods are particularly useful in the case of covariate shift (Shimodaira, 2000), when predictive uncertainty can be used to decide to abstain (Geifman & El-Yaniv, 2017) on ambiguous samples, while still allowing high-certainty predictions. Approaches like MC-Dropout (Gal & Ghahramani, 2016) or Deep Prior Networks (Malinin & Gales, 2018) attempt to tackle this problem, but the uncertainty estimates they provide are often inaccurate on OOD samples (Ovadia et al., 2019). The same problem has been observed for Bayesian Neural Networks (Neal, 1996; Graves, 2011; Blundell et al., 2015), for which sampling efficiently from the posterior over parameters remains challenging for large models (Ovadia et al., 2019).

Transductive learning. Transductive learning (Vapnik, 1998) assumes that the unlabeled test set is available together with a labeled training set and both can be used to select a good predictor. Unlike semi-supervised learning, the transductive framework is only concerned with performing well on the given test set and is not interested in generalization on holdout data. In practice it has been successfully used for problems like zero-shot learning (Fu et al., 2015; Wan et al., 2019). Transductive OOD detection (Scott & Blanchard, 2008) is equivalent to the scenario that we adopt in this paper if the unlabeled set coincides with the test set used for evaluation (see also Appendix F.1).

Domain adaptation. The OOD detection problem with access to unknown OOD data is reminiscent of unsupervised domain adaptation (UDA) (Ben-David et al., 2007; Ganin et al., 2016; Chen et al., 2020), in that both allow access to an unlabeled data set to adjust predictors to a new distribution. However, unlike OOD detection, UDA aims to provide correct predictions on a target distribution with covariate shift (Shimodaira, 2000). Hence, the UDA problem is ill-posed if the target distribution contains data from novel classes, not present in the source set. In novel-class scenarios, one needs to consider OOD detection instead.

B. Theoretical motivation for early stopping regularization

In this section we show how to choose an intermediate checkpoint using the validation set to obtain diverse models that only disagree on OOD samples and not ID samples. This *regularized disagreement* is key to achieving significantly better detection performance on hard OOD tasks than other baselines. We give a rigorous explanation for an ensemble trained from random initializations (i.e. ERD++), but the intuition carries over to ERD fine-tuned from pretrained weights.

Recall that, in our approach, each member of the ensemble tries to fit one label c to the entire unlabeled set U in addition to the correct labels of the ID training set S. Ideally, after training each model with a different label c, we obtain an ensemble of classifiers f_c that disagree only on OOD data. We train the models to fit $S \cup (U, c)$, where we use the notation:

$$(U, c) = (U_{\text{ID}}, c) \cup (U_{\text{OOD}}, c) = \{(x, c) : x \in U_{\text{ID}}\} \cup \{(x, c) : x \in U_{\text{OOD}}\} \tag{1}$$

Moreover, assuming that the labels of the ID data are given by a deterministic function $y^* : \mathcal{X} \to \mathcal{Y}$, we can partition the set (U_{ID}, c) (see Figure 4) into the subset of samples whose ground truth label differs from c and are thus incorrectly labeled

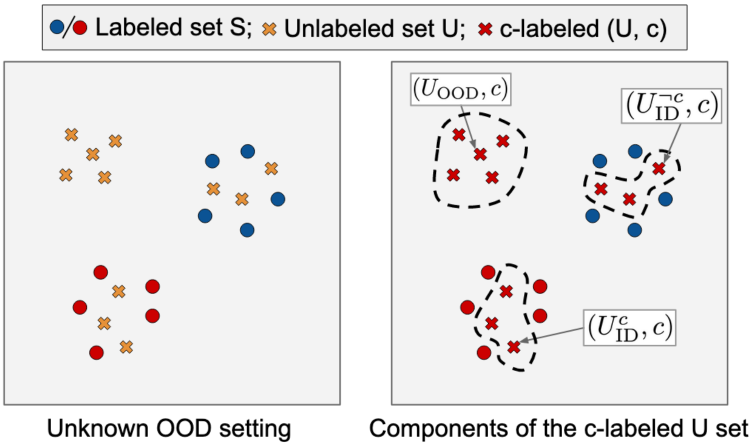
●/● Labeled set S; ✖ Unlabeled set U; ✖ c-labeled (U, c)
(U_{OOD}, c)
$(U_{\mathrm{ID}}^{\neg c}, c)$
(U_{ID}^{c}, c)
Unknown OOD setting
Components of the c-labeled U set

Figure 4. **Left:** Sketch of the *Unknown OOD* setting. **Right:** Illustration of the unlabeled set (U, c) partitioned into (U_{OOD}, c), (U_{ID}^{c}, c), and $(U_{\mathrm{ID}}^{\neg c}, c)$.

with c, and the subset whose correct label is indeed c:

$$(U_{\mathrm{ID}}^{\neg c}, c) := \{(x, c) : x \in U_{\mathrm{ID}} \text{ with } y^*(x) \neq c\} \tag{2}$$
$$(U_{\mathrm{ID}}^{c}, c) := \{(x, c) : x \in U_{\mathrm{ID}} \text{ with } y^*(x) = c\} \tag{3}$$

We now argue that through regularization we can control the model complexity such that the classifier fits S and all of (U, c), except for $(U_{\mathrm{ID}}^{\neg c}, c)$. The *key intuition* why regularization helps is that it is more difficult to fit the labels c on $(U_{\mathrm{ID}}^{\neg c}, c)$ than on (U_{OOD}, c), since $(U_{\mathrm{ID}}^{\neg c}, c)$ lies closer in covariate space to points in the correctly labeled training set S. Hence, we can exactly fit (U_{OOD}, c) but not $(U_{\mathrm{ID}}^{\neg c}, c)$ if we adequately limit the function complexity (e.g. by choosing a small model class, or through regularization), as illustrated in Figure 2 Left. If the models are too complex (e.g. deep neural networks (Zhang et al., 2016)), then they can even fit the wrong labels on $(U_{\mathrm{ID}}^{\neg c}, c)$ (see Figure 2 Right), causing the models in the ensemble to disagree on the entire unlabeled set U.

We use early stopping regularization, motivated by recent empirical and theoretical works that have found that early stopped neural networks are less vulnerable to label noise in the training data(Yilmaz & Heckel, 2019; Li et al., 2020). In particular, we show that for a simple neural network trained with gradient descent there exists a stopping time at which all points in (U, c) are fit, except for $(U_{\mathrm{ID}}^{\neg c}, c)$.

We begin by defining clusterable data sets.

Definition B.1 ((ϵ, ρ)-clusterable data set)**.** *We say that a data set $\mathcal{D} = \{(x_i, y_i)\}_{i=1}^n$ is* (ϵ, ρ)-clusterable *for fixed $\epsilon > 0$ and $\rho \in [0, 1]$ if there exists a partitioning of it into subsets $\{C_1, ..., C_K\}$, which we call* clusters*, each with their associated unit-norm cluster center c_i, that satisfy the following conditions:*

- $\bigcup_{i=1}^K C_i = \mathcal{D}$ *and* $C_i \cap C_j = \emptyset, \forall i, j \in [K]$*;*
- *all the points in a cluster lie in the ϵ-neighborhood of their corresponding cluster center, i.e. $||x - c_i||_2 \leq \epsilon$ for all $x \in C_i$ and all $i \in [K]$;*
- *a fraction of at least $1 - \rho$ of the points in each cluster C_i have the same label, which we call the* cluster label *and denote $y^*(c_i)$. The remaining points suffer from label noise;*
- *if two cluster C_i and C_j have different labels, then their centers are 2ϵ far from each other, i.e. $||c_i - c_j||_2 \geq 2\epsilon$;*
- *the clusters are balanced i.e. for all $i \in [K]$, $\alpha_1 \frac{n}{K} \leq |C_i| \leq \alpha_2 \frac{n}{K}$, where α_1 and α_2 are two positive constants.*

According to this definition, each class may comprise several clusters, but every cluster contains only samples from one class, up to some level of label noise $\rho \in [0, 1]$. In our case, for a fixed label $c \in \mathcal{Y}$, we assume that the set $S \cup (U, c)$ is

(ϵ, ρ)-clusterable into K clusters. We further assume that each cluster C_i only includes a few noisy samples from $(U_{\text{ID}}^{\neg c}, c)$, i.e. $\frac{|C_i \cap (U_{\text{ID}}^{\neg c}, c)|}{|C_i|} \leq \rho$ and that for clusters C_i whose cluster label is not c, i.e. $y^*(c_i) \neq c$, it holds that $C_i \cap (U_{\text{OOD}}, c) = \emptyset$.

We define the matrices $C := [c_1, ..., c_K]^T \in \mathbb{R}^{K \times d}$ and $\Sigma := (CC^T) \bigodot \mathbb{E}_g[\phi'(Cg)\phi'(Cg)^T]$, with $g \sim \mathcal{N}(0, I_d)$ and where $\bigodot$ denotes the elementwise product. We use $\|\cdot\|$ and $\lambda_{min}(\cdot)$ to denote the spectral norm and the smallest eigenvalue of a matrix, respectively.

For prediction, we consider a 2-layer neural network model with p hidden units, where $p \gtrsim \frac{K^2\|C\|^4}{\lambda_{min}(\Sigma)^4}$. We can write this model as follows:

$$x \mapsto f(x; W) = v^T \phi(Wx), \tag{4}$$

The first layer weights W are initialized with random values drawn from $\mathcal{N}(0, 1)$, while the last layer weights v have fixed values: half of them are set to $1/p$ and the other half is $-1/p$. We consider activation functions ϕ with bounded first and second order derivatives, i.e. $|\phi'(x)| \leq \Gamma$ and $\phi''(x) \leq \Gamma$. We use the squared loss for training, i.e. $\mathcal{L}(W) = \frac{1}{2}\sum_{i=0}^{n}(y_i - f(x_i; W))^2$ and take gradient descent steps to find the optimum of the loss function, i.e. $W_{\tau+1} = W_\tau - \eta\nabla\mathcal{L}(W_\tau)$, where the step size is set to $\eta \simeq \frac{K}{n\|C\|^2}$. We can now state the following proposition:

Proposition B.1. *Assume that $\rho \leq \delta/8$ and $\epsilon \leq \alpha\delta\lambda_{min}(\Sigma)^2/K^2$, where δ is a constant such that $\delta \leq \frac{2}{|\mathcal{Y}-1|}$ and α is a constant that depends on Γ. Then it holds with high probability $1 - 3/K^{100} - Ke^{-100d}$ over the initialization of the weights that the neural network trained on $S \cup (U, c)$ perfectly fits S, (U_{ID}^{c}, c) and (U_{OOD}, c), but not $(U_{\text{ID}}^{\neg c}, c)$, after $T = c_4\frac{\|C\|^2}{\lambda_{min}(\Sigma)}$ iterations.*

This result shows that there exists an optimal stopping time at which the neural network predicts the correct label on all ID points and the label c on all the OOD points. As we will see later in the proof, the proposition is derived from a more general result which shows that the early stopped model predicts these labels not only on the points in U but also in an ϵ-neighborhood around cluster centers. Hence, an ERD ensemble can be used to detect holdout OOD samples similar to the ones in U, after being tuned on U. This follows the intuition that classifiers regularized with early stopping are smooth and generalize well.

The clusterable data model is generic enough to include data sets with non-linear decision boundaries. Moreover, notice that the condition in Proposition B.1 is satisfied when $S \cup (U_{\text{ID}}, c)$ is (ϵ, ρ)-clusterable and (U_{OOD}, c) is ϵ-clusterable and if the cluster centers of (U_{OOD}, c) are at distance at least 2ϵ from the cluster centers of $S \cup (U_{\text{ID}}, c)$. A situation in which these requirements are met is, for instance, when the OOD data comes from novel classes, when all classes (including the unseen ones that are not in the training set) are well separated, with cluster centers at least 2ϵ away in Euclidean distance. In addition, in order to limit the amount of label noise in each cluster, it is necessary that the number of incorrectly labeled samples in $(U_{\text{ID}}^{\neg c}, c)$ is small, relative to the size of S.

In practice, we only need that the decision boundary separating (U_{OOD}, c) from S is easier to learn than the classifier required to interpolate the incorrectly labeled $(U_{\text{ID}}^{\neg c}, c)$, which is often the case, provided that (U_{OOD}, c) is large enough and the OOD samples come from novel classes.

We now provide the proof for Proposition B.1:

Proof. We begin by restating a result from (Li et al., 2020):

Theorem B.1 ((Li et al., 2020)). *Let $\mathcal{D} := \{(x_i, y_i)\} \in \mathbb{R}^d \times \mathcal{Y}$ be an (ϵ, ρ)-clusterable training set, with $\epsilon \leq c_1\delta\lambda_{min}(\Sigma)^2/K^2$ and $\rho \leq \delta/8$, where δ is a constant that satisfies $\delta \leq \frac{2}{|\mathcal{Y}|-1}$. Consider a two-layer neural network as described above, and train it with gradient descent starting from initial weights sampled i.i.d. from $\mathcal{N}(0, 1)$. Assume further that the step size is $\eta = c_2\frac{K}{n\|C\|^2}$ and that the number of hidden units p is at least $c_3\frac{K^2\|C\|^4}{\lambda_{min}(\Sigma)^4}$. Under these conditions, it holds with probability at least $1 - 3/K^{100} - Ke^{-100d}$ over the random draws of the initial weights, that after $T = c_4\frac{\|C\|^2}{\lambda_{min}(\Sigma)}$ gradient descent steps, the neural network $x \mapsto f(x; W_T)$ predicts the correct cluster label for all points in the ϵ-neighborhood of the cluster center, namely:*

$$\arg\max_{y\in\mathcal{Y}} |f(x;W_T) - \omega(y)| = y^*(c_i),\ \textit{for all } x \textit{ with } \|x - c_i\|_2 \le \epsilon \textit{ and all clusters } i \in [K], \tag{5}$$

where $\omega : \mathcal{Y} \to \{0,1\}^{|\mathcal{Y}|}$ *yields one-hot embeddings of the labels. The constants* c_1, c_2, c_3, c_4 *depend only on* Γ.

Notice that, under the assumptions introduced above, the set $S \cup (U, c)$ is (ϵ, ρ)-clusterable, since the incorrectly labeled ID points in $(U_{\text{ID}}^{\neg c}, c)$ constitute at most a fraction ρ of the clusters they belong to. As a consequence, Proposition B.1 follows directly from Theorem B.1.

□

C. Disagreement score for OOD detection

As we outlined in Section 3, in this paper we introduce a novel way to aggregate ensemble outputs using a disagreement score. The aggregation metric is tailored to exploit ensemble diversity, which makes it particularly beneficial for ERD. On the other hand, Vanilla Ensembles only rely on the stochasticity of the training process and the random initializations of the weights to produce diverse models, which often leads to classifiers that are strikingly similar as we show in Figure 5 for a few 2D data sets. As a consequence, using our disagreement score $(\text{Avg} \circ \rho)$ for Vanilla Ensembles can sometimes hurt OOD detection performance. To see this, consider the extreme situation in which the models in the ensemble are identical, i.e. $f_1 = f_2$. Then it follows that $(\text{Avg} \circ \rho)(f_1(x), f_2(x)) = 0$, for all test points x and for any function ρ that satisfies the distance axioms.

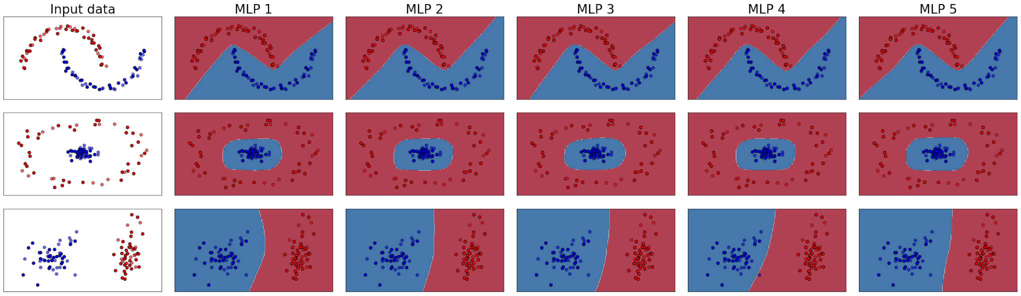

Figure 5. Relying only on the randomness of SGD and of the weight initialization to diversify models is not enough, as it often yields similar classifiers. Each column shows a different predictor trained from random initializations with Adam. All models have the same 1-hidden layer MLP architecture.

Table 2) shows that $(\text{Avg} \circ \rho)$ leads to worse OOD detection performance for Vanilla Ensembles, compared to using the entropy of the average softmax score, $(\text{H} \circ \text{Avg})$, which was proposed in prior work. However, if the ensembles are indeed diverse, as we argue is the case for our method ERD (see Section B), then there is a clear advantage to using a score that, unlike $(\text{H} \circ \text{Avg})$, takes diversity into account, as shown in Table 2.

D. Experiment details

D.1. Baselines

Standard baselines. We compare our method against a wide range of baselines that require different access to OOD data for training, as indicated in Table 3. When it comes to methods that use *no OOD* data for training, the current SOTA on the usual benchmarks is the Gram method (Sastry & Oore, 2019). Other approaches that use no OOD data include vanilla ensembles (Lakshminarayanan et al., 2017), methods that rely on deep generative models (Nalisnick et al., 2019; Choi et al., 2018), which tend to give undesirable results for OOD detection (Kirichenko et al., 2020), or various Bayesian approaches (Gal & Ghahramani, 2016; Blundell et al., 2015) that are often poorly calibrated on OOD data (Ovadia et al., 2019). Moreover, Outlier Exposure (Hendrycks et al., 2019) and Deep Prior Networks (DPN) (Malinin & Gales, 2018) use TinyImages for training as known outliers, irrespective of the OOD set used for evaluation (*Different OOD*). On the other hand, the Mahalanobis baseline (Lee et al., 2018) is tuned on samples from the same OOD distribution used for evaluation.

Table 2. The disagreement score that we propose $(\text{Avg} \circ \rho)$ exploits ensemble diversity and benefits in particular ERD ensembles. OOD detection performance is significantly improved when using $(\text{Avg} \circ \rho)$ compared to the previously proposed $(\text{H} \circ \text{Avg})$ metric. Since Vanilla Ensemble are not diverse enough, a score that relies on model diversity can hurt OOD detection performance. We highlight the AUROC and the TNR@95 obtained with the score function that is ***best for Vanilla Ensemble*** and the **best for ERD**.

ID data	OOD data	Vanilla Ensembles $(\text{H} \circ \text{Avg})$	Vanilla Ensembles $(\text{Avg} \circ \rho)$	ERD $(\text{H} \circ \text{Avg})$	ERD $(\text{Avg} \circ \rho)$
		AUROC ↑ / TNR@95 ↑			
SVHN	CIFAR10	***0.97*** / ***0.88***	0.96 / ***0.89***	0.86 / 0.85	**0.99** / **0.97**
CIFAR10	SVHN	***0.92*** / ***0.78***	0.91 / ***0.78***	0.92 / 0.92	**1.00** / **1.00**
CIFAR100	SVHN	***0.84*** / ***0.48***	0.79 / 0.46	0.36 / 0.35	**1.00** / **1.00**
SVHN[0:4]	SVHN[5:9]	***0.92*** / ***0.69***	0.91 / ***0.69***	**0.94** / **0.66**	**0.94** / **0.66**
CIFAR10[0:4]	CIFAR10[5:9]	***0.80*** / ***0.39***	***0.80*** / ***0.39***	**0.91** / 0.65	**0.91** / **0.66**
CIFAR100[0:49]	CIFAR100[50:99]	***0.78*** / ***0.35***	0.76 / 0.34	0.63 / 0.38	**0.81** / **0.40**
Average		***0.87*** / ***0.60***	0.86 / 0.59	0.77 / 0.64	**0.94** / **0.78**

Table 3. Related OOD detection methods and the OOD data that they use.

Baseline	Access to OOD
Vanilla Ensemble (Lakshminarayanan et al., 2017)	No OOD
Gram method (Sastry & Oore, 2019)	No OOD
Generative (Nalisnick et al., 2019; Choi et al., 2018)	No OOD
nnPU (Kiryo et al., 2017)	Unknown OOD
MCD (Yu & Aizawa, 2019)	Unknown OOD
ERD (Ours)	Unknown OOD
Outlier Exposure (Hendrycks et al., 2019)	Different OOD
DPN (Malinin & Gales, 2018)	Different OOD
ODIN (Liang et al., 2018)	Oracle OOD
Mahalanobis (Lee et al., 2018)	Oracle OOD

Unknown OOD and PU learning. We also compare our method to approaches that assume the same setting, in which an unlabeled set with ID and OOD samples is available. The recently proposed MCD method (Yu & Aizawa, 2019) trains an ensemble of two classifiers with different types of predictive distributions on the unlabeled samples: one model gives high-entropy predictions, while the other has low entropy. Furthermore, positive-unlabeled (PU) learning (du Plessis et al., 2014) considers a binary classification setting, in which the labeled data comes from one class (i.e. ID samples, in our case), while the unlabeled set contains a mixture of samples from both classes. Crucially, PU learning methods, like nnPU (Kiryo et al., 2017), require oracle knowledge of the ratio of OOD samples in the unlabeled set.

Unknown OOD – new baselines. In addition to these methods, we propose two more baselines that use an unlabeled set. Firstly, we present a version of the Mahalanobis approach (*Mahal-U*) that is calibrated using the unlabeled set. Secondly, since PU learning requires access to the OOD ratio of the unlabeled set, we also consider a less burdensome alternative: a binary classifier trained to separate the training data from the unlabeled set and regularized with early stopping like our method.

D.2. Tuning hyperparameters

For all baselines we use the hyperparameters suggested by the authors for the respective data sets (e.g. different hyperparameters for CIFAR10 or ImageNet). For all methods, we use pretrained models provided by the authors. However, we note that for the novel-class settings, pretraining on the entire training set means that the model is exposed to the OOD classes as well, which is undesirable. Therefore, for these settings we pretrain only on the split of the training set that contains the ID classes. Since the classification problem is similar to the original one of training on the entire training set, we use the same hyperparameters that the authors report in the original papers.

Moreover, we point out that even though different methods use different model architectures, that is not inherently unreasonable when the goal is OOD detection, since it is not clear if a complex model is more desirable than a smaller model. For this reason, we use the model architecture recommended by the authors of the baselines and which was used to produce the good results reported in their published works. For Vanilla Ensembles and for ERD we show results for different architectures in Appendix F.6.

- **Vanilla Ensembles** (Lakshminarayanan et al., 2017): We train an ensemble on the training set according to the true labels. For a test sample, we average the outputs of the softmax probabilities predicted by the models, and use the entropy of the resulting distribution as the score for the hypothesis test described in Section 3. We use ensembles of 5 models, with the same architecture and hyperparameters as the ones used for ERD. Hyperparameters are tuned to achieve good validation accuracy.

- **Gram method** (Sastry & Oore, 2019): The Gram baseline is similar to the Mahalanobis method in that both use the intermediate feature representations obtained with a deep neural network to determine whether a test point is an outlier. However, what sets the Gram method apart is the fact that it does not need any OOD data for training or calibration. We use the pretrained models provided by the authors, or train our own, using the same methodology as described for the Mahalanobis baseline. For OOD detection, we use the code published by the authors. We note that for MLP models, the Gram method is difficult to tune and we could not find a configuration that works well, despite our best efforts and following the suggestions proposed during our communication with the authors.

- **Deep Prior Networks (DPN)** (Malinin & Gales, 2018): DPN is a Bayesian Method that trains a neural network (Prior Network) to parametrize a Dirichlet distribution over the class probabilities. We train a WideResNet WRN-28-10 for 100 epochs using SGD with momentum 0.9, with an initial learning rate of 0.01, which is decayed by 0.2 at epochs 50, 70, and 90. For MNIST, we use EMINST/Letters as OOD for tuning. For all other settings, we use TinyImages as OOD for tuning.

- **Outlier Exposure** (Hendrycks et al., 2019): This approach makes a model's softmax predictions close to the uniform distribution on the known outliers, while maintaining a good classification performance on the training distribution. We use the WideResNet architecture (WRN) (Zagoruyko & Komodakis, 2016). For fine-tuning, we use the settings recommended by the authors, namely we train for 10 epochs with learning rate 0.001. For training from scratch, we train for 100 epochs with an initial learning rate of 0.1. When the training data set is either CIFAR10/CIFAR100 or ImageNet, we use the default WRN parameters of the author's code, namely 40 layers, 2 widen-factor, droprate 0.3. When the training dataset is SVHN, we use the author's recommended parameters of 16 layers, 4 widen-factor and droprate 0.4. All settings use the cosine annealing learning rate scheduler provided with the author's code, without any modifications. For all settings, we use TinyImages as known OOD data during training. In Section F.4 we show results for known OOD data that is similar to the OOD data used for testing.

- **Mahalanobis** (Lee et al., 2018): The method pretrains models on the labeled training data. For a test data point, it uses the intermediate representations of each layer as "extracted features". It then performs binary classification using logistic regression using these extracted features. In the original setting, the classification is done on "training" ID vs "training" OOD samples (which are from the same distribution as the test OOD samples). Furthermore, hyperparameter tuning for the optimal amount of noise is performed on validation ID and OOD data. We use the WRN-28-10 architecture, pretrained for 200 epochs. The initial learning rate is 0.1, which is decayed at epochs 60, 120, and 160 by 0.2. We use SGD with momentum 0.9, and the standard weight decay of $5 \cdot 10^{-4}$. The code published for the Mahalanobis method performs a hyperparameter search automatically for each of the data sets.

The following baselines assume the same *Unknown OOD* setting as ERD, in which one has access to both a labeled ID training set S and an unlabeled set with an unknown mixture of ID and OOD samples U.

- **Non-negative PU learning (nnPU)** (Kiryo et al., 2017): The method trains a binary predictor to distinguish between a set of known positives (in our case the ID data) and a set that contains a mixture of positives and negatives (in our case the unlabeled set). To prevent the interpolation of all the unlabeled samples, (Kiryo et al., 2017) proposes a regularized objective. It is important to note that most training objectives in the PU learning literature require that the ratio between the positives and negatives in the unlabeled set is known or easy to estimate. For our experiments we always use the exact OOD ratio to train the nnPU baseline. Therefore, we obtain an upper bound on the AUROC/TNR@95. If the ratio is estimated from finite samples, then estimation errors may lead to slightly worse OOD detection performance. We perform a grid search over the learning rate and the threshold that appears in the nnPU regularizer and pick the option with the best validation accuracy measured on a holdout set with only positive samples (in our case, ID data).

- **Maximum Classifier Discrepancy (MCD)** (Yu & Aizawa, 2019): The MCD method trains two classifiers at the same time, and makes them disagree on the unlabeled data, while maintaining good classification performance. We use the

WRN-28-10 architecture as suggested in the paper. We did not change the default parameters which came with the author's code, so weight decay is 10^{-4}, and the optimizer is SGD with momentum 0.9. When available (for CIFAR10 and CIFAR100), we use the pretrained models provided by the authors. For the other training datasets, we use their methodology to generate pretrained models: We train a WRN-28-10 for 200 epochs. The learning rate starts at 0.1 and drops by a factor of 10 at 50% and 75% of the training progress.

- **Mahalanobis-U**: This is a slightly different version of the Mahalanobis baseline, for which we use early-stopped logistic regression to distinguish between the training set and an unlabeled set with ID and OOD samples (instead of discriminating a known OOD set from the inliers). The early stopping iteration is chosen to minimize the classification errors on a validation set that contains only ID data (recall that we do not assume to know which are the OOD samples).

In addition to these approaches that have been introduced in prior work, we also propose a strong novel baseline that that bares some similarity to PU learning and to ERD.

- **Binary classifier** The approach consists in discriminating between the labeled ID training set and the mixed unlabeled set, that contains both ID and OOD data. We use regularization to prevent the trivial solution for which the entire unlabeled set is predicted as OOD. Unlike PU learning, the binary classifier does not require that the OOD ratio in the test distribution is known. The approach is similar to a method described in (Scott & Blanchard, 2008) which also requires that the OOD ratio of the unlabeled set is known. We tune the learning rate and the weight of the unlabeled samples in the training loss by performing a grid search and selecting the configuration with the best validation accuracy, computed on a holdout set containing only ID samples. We note that the binary classifier that appears in Section G in the medical benchmark, is not the same as this baseline. For more details on the binary classifier that appears in the medical data experiments we refer the reader to (Cao et al., 2020).

D.3. Training configuration for ERD

For ERD we always use hyperparameters that give the best validation accuracy when training a model on the ID training set. In other words, we pick hyperparameter values that lead to good ID generalization and do not perform further hyperparameter tuning for the different OOD data sets on which we evaluate our approach.

For MNIST and FashionMNIST, we train ensembles of 3-layer MLP models with ReLU activations. Each intermediate layer has 100 neurons. The models are optimized using Adam, with a learning rate of 0.001, for 10 epochs.

For SVHN, CIFAR10/CIFAR100 and ImageNet, we train ensembles of ResNet20 (He et al., 2016). The models are initialized with weights pretrained for 100 epochs on the labeled training set. We fine-tune each model for 10 epochs using SGD with momentum 0.9, and a learning rate of 0.001. The weights are trained with an ℓ_2 regularization coefficient of $5e-4$. We use a batch size of 128 for all scenarios, unless explicitly stated otherwise. We used the same hyperparameters for all settings.

For pretraining, we perform SGD for 100 epochs and use the same architecture and hyperparameters as described above, with the exception of the learning rate that starts at 0.1, and is multiplied by 0.2 at epochs 50, 70 and 90.

Apart from ERD, which fine-tunes the ensemble models starting from pretrained weights, we also present in the Appendix results for ERD++. This variant of our method trains the models from random initializations, and hence needs more iterations to converge, making it more computationally expensive than ERD. We train all models in the ERD++ ensembles for 100 epochs with a learning rate that starts at 0.1, and is multiplied by 0.2 at epochs 50, 70 and 90. All other hyperparameters are the same as for ERD ensembles.

For the medical data sets, we train a Densenet-121 as the authors do in the original paper (Cao et al., 2020). For ERD++, we do not use random weight initializations, but instead we start with the ImageNet weights provided with Tensorflow. The training configuration is exactly the same as for ResNet20, except that we use a batch size of 32 due to GPU memory restrictions, and for fine tuning we use a constant learning rate of 10^{-5}.

Computation cost. For ERD as few as three epochs of fine-tuning are enough on average to achieve the performance that we report. This amounts to around 2 minutes if the models in the ensemble are fine-tuned in parallel on NVIDIA GeForce GTX 1080 Ti GPUs.

E. ID and OOD data sets

E.1. Data sets

For evaluation, we use the following image data sets: MNIST (Lecun et al., 1998), Fashion MNIST (Xiao et al., 2017), SVHN (Netzer et al., 2011), CIFAR10 and CIFAR100 (Krizhevsky, 2009).

For the experiments using MNIST and FashionMNIST the training set size is 50K, the validation size is 10K, and the test ID and test OOD sizes are both 10K. For SVHN, CIFAR10 and CIFAR100, the training set size is 40K, the validation size is 10K, and the unlabeled set contains 10K samples: 5K are ID and 5K are OOD. For evaluation, we use a holdout set of 10K examples (half ID, half OOD). For the settings that use half of the classes as ID and the other half as OOD, all the sizes are divided by 2.

E.2. Samples for the settings with novel classes

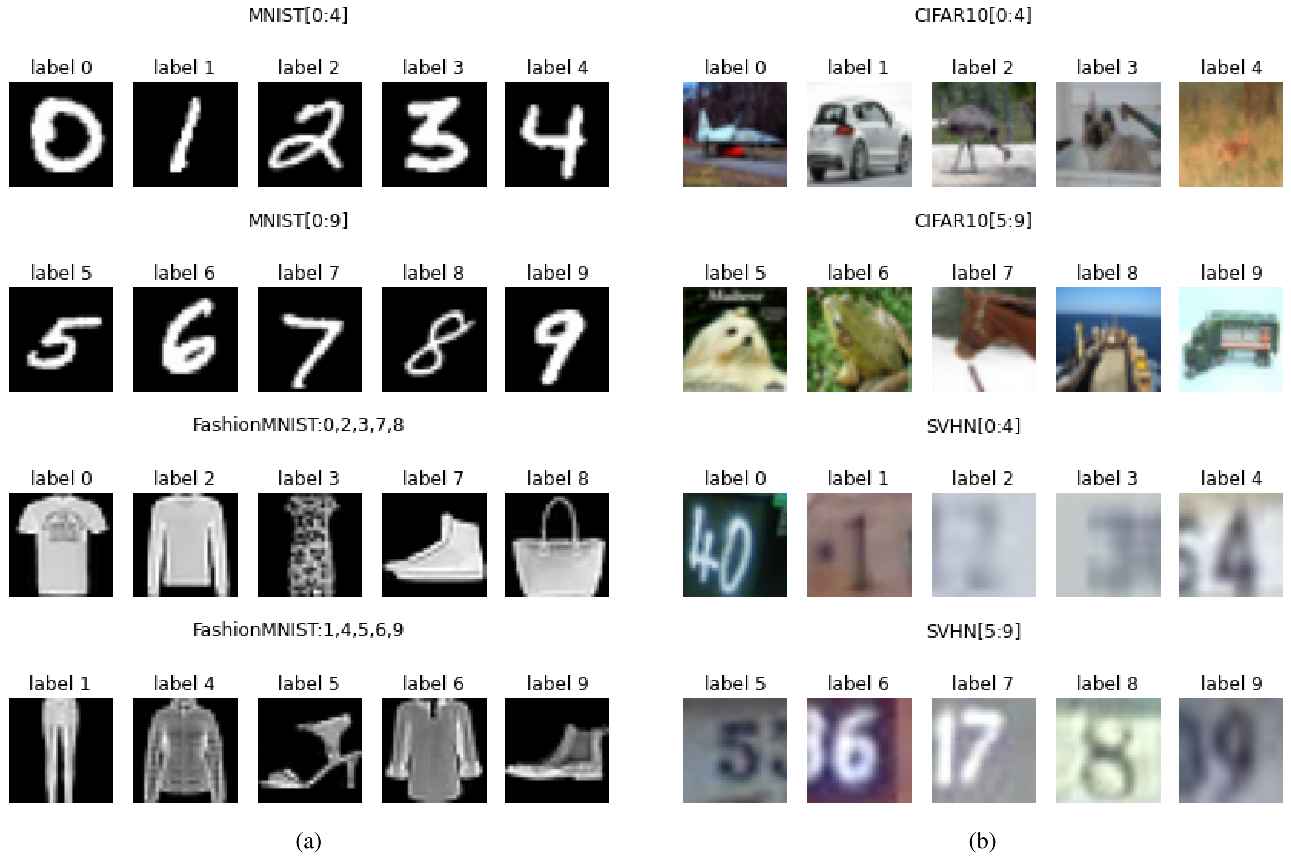

(a)

(b)

Figure 6. (a) Data samples for the MNIST/FashionMNIST splits. (b) Data samples for the CIFAR10/SVHN splits.

F. More experiments

F.1. Evaluation on the unlabeled set

In the main text we describe how one can leverage the unlabeled set U to obtain an OOD detection algorithm that accurately identifies outliers at test time that similar to the ones in U. It is, however, possible to also use our method ERD to flag the OOD samples contained in the same set U used for fine-tuning the ensemble. In Table 4 we show that the OOD detection performance of ERD is similar regardless of whether we use U for evaluation, or a holdout test set T drawn from the same distribution as U.

Table 4. Comparison between the OOD detection performance of ERD when using a holdout test set T for evaluation, or the same unlabeled set U that was used for fine-tuning the models.

ID data	OOD data	ERD (eval on T)	ERD (eval on U)
		AUROC ↑ / TNR@95 ↑	
SVHN	CIFAR10	1.00 / 0.99	1.00 / 0.99
CIFAR10	SVHN	1.00 / 1.00	1.00 / 1.00
CIFAR100	SVHN	1.00 / 1.00	1.00 / 1.00
FMNIST[0,2,3,7,8]	FMNIST[1,4,5,6,9]	0.94 / 0.67	0.94 / 0.67
SVHN[0:4]	SVHN[5:9]	0.95 / 0.74	0.96 / 0.79
CIFAR10[0:4]	CIFAR10[5:9]	0.93 / 0.70	0.93 / 0.69
CIFAR100[0:49]	CIFAR100[50:99]	0.82 / 0.44	0.80 / 0.36
Average		0.95 / 0.79	0.95 / 0.79

F.2. OOD detection for data with covariate shift

In this section we evaluate the baselines and the method that we propose on settings in which the OOD data suffers from covariate shift (Shimodaira, 2000). The goal is to identify all samples that come from the shifted distribution, regardless of how strong the shift is. Notice that mild shifts may be easier to tackle by domain adaptation algorithms, but when the goal is OOD detection they pose a much more difficult challenge.

We want to stress that in practice one may not be interested in identifying *all* samples with distribution shift as OOD, since a classifier may still produce correct predictions on some of them. In contrast, when data suffers from covariate shift we can try to learn predictors that perform well on both the training and the test distribution, and we may use a measure of predictive uncertainty to identify only those test samples on which the classifier cannot make confident predictions. Nevertheless, we use these covariate shift settings as a challenging OOD detection benchmark and show in Table 6 that our method ERD does indeed outperform prior baselines on these difficult settings.

We use as outliers corrupted variants of CIFAR10 and CIFAR100 (Hendrycks & Dietterich, 2019), as well as a scenario where ImageNet (Deng et al., 2009) is used as ID data and ObjectNet (Barbu et al., 2019) as OOD, both resized to 32x32. Figure 7 shows samples from these data sets. The Gram and nnPU baselines do not give satisfactory results on the difficult CIFAR10/CIFAR100 settings in Table 1 and thus we do not consider them for the distribution shift cases. For the *Unknown OOD* methods (i.e. MCD, Mahal-U and ERD/ERD++) we evaluate on the same unlabeled set that is used for training (see the discussion in Section F.1).

Furthermore, we present results on distinguishing between CIFAR10 (Krizhevsky, 2009) and CIFAR10v2 (Recht et al., 2018), a data set meant to be drawn from the same distribution as CIFAR10 (generated from the Tiny Images collection (Torralba et al., 2008)). In (Recht et al., 2019), the authors argue that CIFAR10 and CIFAR10v2 come from very similar distributions. They provide supporting evidence by training a binary classifier to distinguish between them, and observing that the accuracy that is obtained of 52.9% is very close to random.

Our experiments show that the two data sets are actually distinguishable, contrary to what previous work has argued. First, our own binary classifier trained on CIFAR10 vs CIFAR10v2 obtains a test accuracy of 67%, without any hyperparameter tuning. The model we use is a ResNet20 trained for 200 epochs using SGD with momentum 0.9. The learning rate is decayed by 0.2 at epochs 90, 140, 160 and 180. We use 1600 examples from each data set for training, and we validate using 400 examples from each data set.

Table 5. OOD detection performance on CIFAR10 vs CIFAR10v2

ID data	OOD data	Vanilla Ensembles	DPN	OE	Mahal.	MCD	Mahal-U	ERD	ERD++
					AUROC ↑ / TNR@95 ↑				
CIFAR10	CIFAR10v2	***0.64*** / ***0.13***	0.63 / 0.09	***0.64*** / 0.12	0.55 / 0.08	0.58 / 0.10	0.56 / 0.07	0.76 / 0.26	**0.91** / **0.80**

Our OOD detection experiments (presented in Table 5) show that most baselines are able to distinguish between the two data sets, with ERD achieving the highest performance. The methods which require OOD data for tuning (Outlier Exposure and DPN) use CIFAR100.

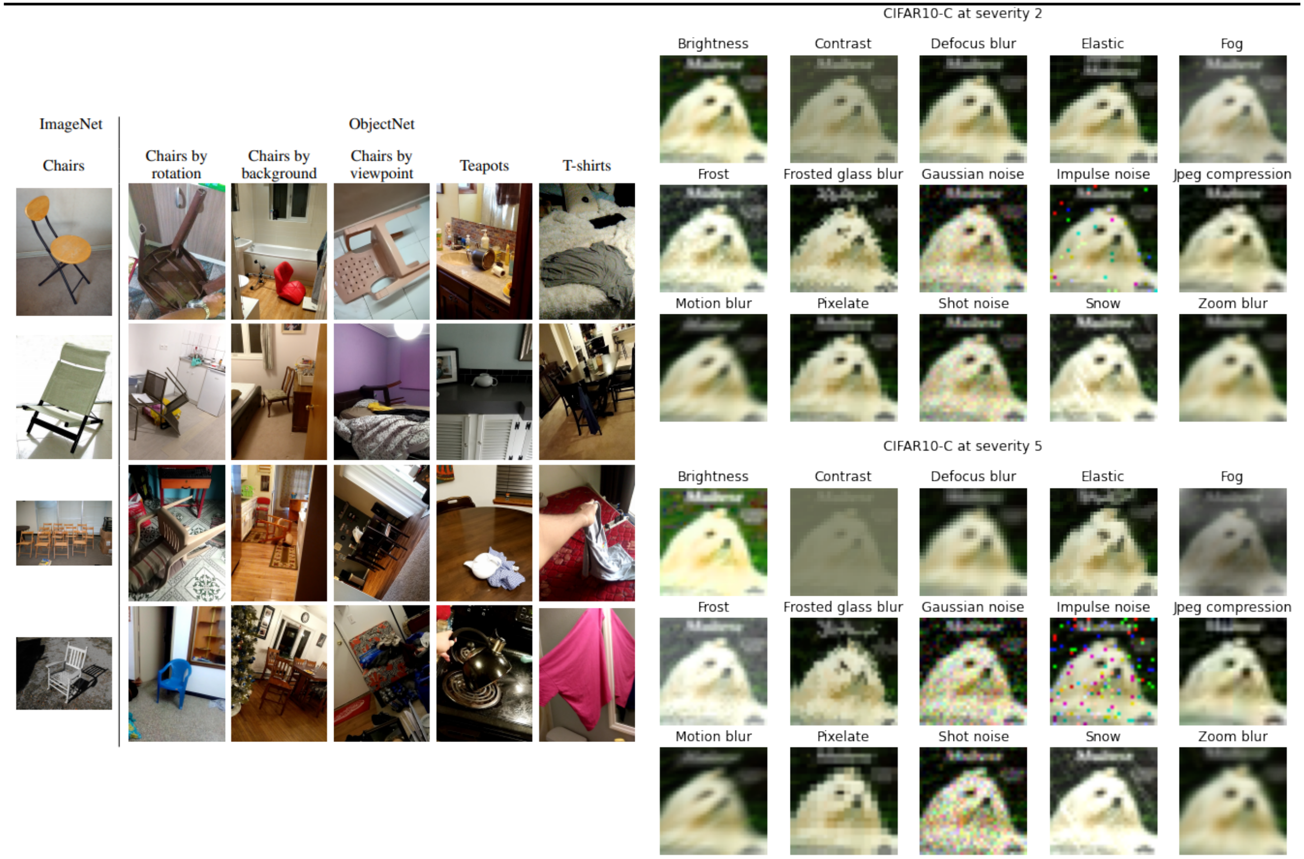

Figure 7. Left: Samples from ImageNet and ObjectNet taken from the original paper by (Barbu et al., 2019). Right: Data samples for the corrupted CIFAR10-C data set.

Table 6. OOD detection performance on data with covariate shift. For ERD and vanilla ensembles, we train 5 ResNet20 models for each setting. The evaluation metrics are computed on the unlabeled set.

ID data	OOD data	Vanilla Ensembles	DPN	OE	Mahal.	MCD	Mahal-U	ERD	ERD++
					AUROC ↑ / TNR@95 ↑				
CIFAR10	CIFAR10-C sev 2 (A)	0.68 / 0.20	0.73 / 0.31	0.70 / 0.20	*0.84* / *0.53*	0.82 / 0.50	0.75 / 0.38	0.96 / 0.86	**0.99** / **0.95**
CIFAR10	CIFAR10-C sev 2 (W)	0.51 / 0.05	0.47 / 0.03	0.52 / 0.06	*0.58* / *0.08*	0.52 / 0.06	0.55 / 0.07	0.68 / 0.19	**0.86** / **0.41**
CIFAR10	CIFAR10-C sev 5 (A)	0.84 / 0.49	0.89 / 0.60	0.86 / 0.54	0.94 / 0.80	*0.95* / *0.84*	0.88 / 0.63	**1.00** / 0.99	**1.00** / **1.00**
CIFAR10	CIFAR10-C sev 5 (W)	0.60 / 0.10	0.72 / 0.10	0.63 / 0.11	*0.78* / *0.27*	0.60 / 0.08	0.68 / 0.12	0.98 / 0.86	**1.00** / **1.00**
CIFAR100	CIFAR100-C sev 2 (A)	0.68 / 0.20	0.62 / 0.18	0.65 / 0.19	*0.82* / *0.48*	0.72 / 0.29	0.67 / 0.22	0.94 / 0.76	**0.97** / **0.86**
CIFAR100	CIFAR100-C sev 2 (W)	0.52 / 0.06	0.32 / 0.03	0.52 / 0.06	*0.55* / *0.07*	0.52 / 0.06	0.55 / 0.06	0.71 / 0.19	**0.86** / **0.44**
CIFAR100	CIFAR100-C sev 5 (A)	0.78 / 0.37	0.74 / 0.36	0.76 / 0.37	*0.92* / *0.72*	0.91 / 0.65	0.84 / 0.55	0.99 / 0.97	**1.00** / **0.99**
CIFAR100	CIFAR100-C sev 5 (W)	0.64 / 0.14	0.49 / 0.12	0.62 / 0.13	*0.71* / *0.19*	0.60 / 0.10	0.63 / 0.13	0.96 / 0.71	**0.98** / **0.89**
Tiny ImageNet	Tiny ObjectNet	0.82 / 0.49	0.70 / 0.32	0.79 / 0.37	0.75 / 0.26	*0.99* / *0.98*	0.72 / 0.25	0.98 / 0.88	**0.99** / **0.98**
	Average	0.67 / 0.23	0.63 / 0.23	0.67 / 0.23	*0.76* / 0.38	0.74 / *0.39*	0.70 / 0.27	0.91 / 0.71	**0.96** / **0.83**

F.3. Results with a smaller unlabeled set

We now show that our method performs well even when the unlabeled set is significantly smaller. In particular, we show in the table below that ERD maintains a high AUROC and TNR@95 even when only 1,000 unlabeled samples are used for fine-tuning (500 ID and 500 OOD).

Table 7. Experiments with a test set of size 1,000, with an equal number of ID and OOD test samples. For ERD and vanilla ensembles, we train 5 ResNet20 models for each setting. The evaluation metrics are computed on the unlabeled set.

ID data	OOD data	Vanilla Ensembles	DPN	OE	Mahal.	MCD	Mahal-U	ERD
					AUROC ↑ / TNR@95 ↑			
SVHN	CIFAR10	0.97 / 0.88	***1.00*** / ***1.00***	***1.00*** / ***1.00***	0.99 / 0.98	0.97 / 0.85	0.99 / 0.95	**1.00** / **0.99**
CIFAR10	SVHN	0.92 / 0.78	0.95 / 0.85	0.97 / 0.89	***0.99*** / ***0.96***	1.00 / 0.98	0.99 / 0.96	**1.00** / **1.00**
CIFAR100	SVHN	0.84 / 0.48	0.77 / 0.44	0.82 / 0.50	***0.98*** / ***0.90***	0.97 / 0.73	0.98 / 0.92	**0.99** / **1.00**
SVHN[0:4]	SVHN[5:9]	***0.92*** / 0.69	0.87 / 0.19	0.85 / 0.52	***0.92*** / ***0.71***	0.91 / 0.51	0.91 / 0.63	**0.97** / **0.86**
CIFAR10[0:4]	CIFAR10[5:9]	0.80 / 0.39	***0.82*** / 0.32	***0.82*** / ***0.41***	0.79 / 0.27	0.69 / 0.25	0.64 / 0.13	**0.87** / **0.50**
CIFAR100[0:49]	CIFAR100[50:99]	***0.78*** / ***0.35***	0.70 / 0.26	0.74 / 0.31	0.72 / 0.20	0.70 / 0.26	0.72 / 0.19	**0.79** / **0.38**
CIFAR10	CIFAR10-C sev 2 (A)	0.68 / 0.20	0.73 / 0.31	0.70 / 0.20	***0.84*** / ***0.53***	0.82 / 0.50	0.75 / 0.38	**0.91** / **0.71**
CIFAR10	CIFAR10-C sev 2 (W)	0.51 / 0.05	0.47 / 0.03	0.52 / 0.06	***0.58*** / ***0.08***	0.52 / 0.06	0.55 / 0.07	**0.57** / **0.09**
CIFAR10	CIFAR10-C sev 5 (A)	0.84 / 0.49	0.89 / 0.60	0.86 / 0.54	***0.94*** / ***0.80***	0.95 / 0.84	0.88 / 0.63	**0.99** / **0.95**
CIFAR10	CIFAR10-C sev 5 (W)	0.60 / 0.10	0.72 / 0.10	0.63 / 0.11	***0.78*** / ***0.27***	0.60 / 0.08	0.68 / 0.12	**0.92** / **0.67**
CIFAR100	CIFAR100-C sev 2 (A)	0.68 / 0.20	0.62 / 0.18	0.65 / 0.19	***0.82*** / ***0.48***	0.72 / 0.29	0.67 / 0.22	**0.84** / **0.48**
CIFAR100	CIFAR100-C sev 2 (W)	0.52 / 0.06	0.32 / 0.03	0.52 / 0.06	***0.55*** / ***0.07***	0.52 / 0.06	**0.55** / 0.06	**0.55** / **0.07**
CIFAR100	CIFAR100-C sev 5 (A)	0.78 / 0.37	0.74 / 0.36	0.76 / 0.37	***0.92*** / ***0.72***	0.91 / 0.65	0.84 / 0.55	**0.96** / **0.80**
CIFAR100	CIFAR100-C sev 5 (W)	0.64 / 0.14	0.49 / 0.12	0.62 / 0.13	***0.71*** / ***0.19***	0.60 / 0.10	0.63 / 0.13	**0.81** / **0.25**
	Average	0.75 / 0.37	0.72 / 0.34	0.75 / 0.38	***0.82*** / ***0.51***	0.78 / 0.44	0.77 / 0.42	**0.87** / **0.62**

F.4. More results for Outlier Exposure

Table 8. Results for Outlier Exposure, when using the same corruption type, but with a higher/lower severity, as OOD data seen during training.

ID data	OOD data	OE (trained on sev5)	OE (trained on sev2)
		AUROC ↑	
CIFAR10	CIFAR10-C sev 2 (A)	0.89	N/A
CIFAR10	CIFAR10-C sev 2 (W)	0.65	N/A
CIFAR10	CIFAR10-C sev 5 (A)	N/A	0.98
CIFAR10	CIFAR10-C sev 5 (W)	N/A	0.78
CIFAR100	CIFAR100-C sev 2 (A)	0.85	N/A
CIFAR100	CIFAR100-C sev 2 (W)	0.59	N/A
CIFAR100	CIFAR100-C sev 5 (A)	N/A	0.97
CIFAR100	CIFAR100-C sev 5 (W)	N/A	0.67
	Average	0.87	0.98

The Outlier Exposure method needs access to a set of OOD samples during training. The numbers we report in the rest of paper for Outlier Exposure are obtained by using the TinyImages data set as the OOD samples that are seen during training. In this section we explore the use of an $\mathrm{OOD}_{\mathrm{train}}$ data set that is more similar to the OOD data observed at test time. This is a much easier setting for the Outlier Exposure method: the closer $\mathrm{OOD}_{\mathrm{train}}$ is to $\mathrm{OOD}_{\mathrm{test}}$, the easier it will be for the model tuned on $\mathrm{OOD}_{\mathrm{train}}$ to detect the test OOD samples.

In Table 8 we focus only on the settings with corruptions. For each corruption type, we use the lower severity corruption as $\mathrm{OOD}_{\mathrm{train}}$ and evaluate on the higher severity data and vice versa. We report for each metric the average taken over all corruptions (A), and the value for the worst-case setting (W).

F.5. Results on MNIST and FashionMNIST

Table 9. Results on MNIST/FashionMNIST settings. For ERD and vanilla ensembles, we train 5 3-hidden layer MLP models for each setting. The evaluation metrics are computed on the unlabeled set.

ID data	OOD data	Vanilla Ensembles	DPN	OE	Mahal.	nnPU	MCD	Mahal-U	Bin. Classif.	ERD	ERD++
						AUROC ↑ / TNR@95 ↑					
MNIST	FMNIST	0.81 / 0.01	***1.00*** / ***1.00***	***1.00*** / ***1.00***	***1.00*** / ***1.00***	***1.00*** / ***1.00***	***1.00*** / 0.98	***1.00*** / ***1.00***	1.00 / 1.00	**1.00** / **1.00**	**1.00** / **1.00**
FMNIST	MNIST	0.87 / 0.42	***1.00*** / ***1.00***	0.68 / 0.16	0.99 / 0.97	***1.00*** / ***1.00***	***1.00*** / ***1.00***	0.99 / 0.96	1.00 / 1.00	**1.00** / **1.00**	**1.00** / **1.00**
MNIST[0:4]	MNIST[5:9]	0.94 / 0.72	***0.99*** / 0.97	0.95 / 0.78	***0.99*** / ***0.98***	***0.99*** / 0.97	0.96 / 0.76	***0.99*** / ***0.98***	0.99 / 0.94	**0.99** / 0.96	**0.99** / **0.97**
FMNIST[0,2,3,7,8]	FMNIST[1,4,5,6,9]	0.64 / 0.07	0.77 / 0.15	0.66 / 0.12	0.77 / 0.20	***0.95*** / ***0.71***	0.78 / 0.30	0.82 / 0.39	0.95 / 0.66	**0.94** / 0.67	**0.94** / **0.68**
Average		0.82 / 0.30	0.94 / 0.78	0.82 / 0.51	0.94 / 0.79	***0.98*** / ***0.92***	0.94 / 0.76	0.95 / 0.83	0.98 / 0.90	**0.98** / **0.91**	**0.98** / **0.91**

For FashionMNIST we chose this particular split (i.e. classes 0,2,3,7,8 vs classes 1,4,5,6,9) because the two partitions are more similar to each other. This makes OOD detection more difficult than the 0-4 vs 5-9 split.

F.6. Vanilla and ERD Ensembles with different architectures

In this section we present OOD detection results for Vanilla and ERD ensembles with different architecture choices, and note that the better performance of our method is maintained across model classes. Moreover, we observe that ERD benefits from employing more complex models, like the WideResNet.

Table 10. Results with three different architectures for Vanilla and ERD ensembles. All ensembles comprise 5 models. For the corruption data sets, we report for each metric the average taken over all corruptions (A), and the value for the worst-case setting (W). The evaluation metrics are computed on the unlabeled set.

		VGG16		ResNet20		WideResNet-28-10	
ID data	OOD data	Vanilla Ensembles	ERD	Vanilla Ensembles	ERD	Vanilla Ensembles	ERD
				AUROC ↑ / TNR@95 ↑			
SVHN	CIFAR10	0.97 / 0.88	0.99 / 0.94	0.97 / 0.88	0.99 / 0.97	0.96 / 0.86	1.00 / 0.99
CIFAR10	SVHN	0.88 / 0.69	1.00 / 1.00	0.92 / 0.78	1.00 / 1.00	0.94 / 0.81	1.00 / 1.00
SVHN[0:4]	SVHN[5:9]	0.89 / 0.60	0.93 / 0.63	0.92 / 0.69	0.94 / 0.66	0.91 / 0.62	0.96 / 0.78
CIFAR10[0:4]	CIFAR10[5:9]	0.74 / 0.29	0.91 / 0.63	0.80 / 0.39	0.91 / 0.66	0.80 / 0.35	0.94 / 0.71
CIFAR10	CIFAR10-C sev 2 (A)	0.66 / 0.17	0.94 / 0.79	0.68 / 0.20	0.96 / 0.86	0.69 / 0.18	0.98 / 0.90
CIFAR10	CIFAR10-C sev 2 (W)	0.51 / 0.05	0.68 / 0.19	0.51 / 0.05	0.68 / 0.19	0.51 / 0.05	0.84 / 0.35
CIFAR10	CIFAR10-C sev 5 (A)	0.80 / 0.41	0.99 / 0.96	0.84 / 0.49	1.00 / 0.99	0.84 / 0.47	1.00 / 1.00
CIFAR10	CIFAR10-C sev 5 (W)	0.58 / 0.10	0.95 / 0.72	0.60 / 0.10	0.98 / 0.86	0.59 / 0.09	0.99 / 0.97
Average		0.75 / 0.40	0.92 / 0.73	0.78 / 0.45	0.93 / 0.77	0.78 / 0.43	0.96 / 0.84

G. Medical OOD detection benchmark

The medical OOD detection benchmark is organized as follows. There are four training (ID) data sets, from three different domains: two data sets with chest X-rays, one with fundus imaging and one with histology images. For each ID data set, the authors consider three different OOD scenarios:

1. Use case 1: The OOD data set contains images from a completely different domain, similar to our category of easy OOD detection settings.
2. Use case 2: The OOD data set contains images with various corruptions, similar to the hard covariate shift settings that we consider in Section F.2.
3. Use case 3: The OOD data set contains images that come from novel classes, not seen during training.

The authors evaluate a number of methods on all these scenarios. The methods can be roughly categorized as follows:

1. Data-only methods: Fully non-parametric approaches like kNN.

2. Classifier-only methods: Methods that use a classifier trained on the training set, e.g. ODIN (Liang et al., 2018), Mahalanobis (Lee et al., 2018). ERD falls into this category as well.

3. Methods with Auxiliary Models: Methods that use an autoencoder or a generative model, like a Variational Autoencoder or a Generative Adversarial Network. Some of these approaches can be expensive to train and difficult to optimize and tune.

We stress the fact that for most of these methods the authors use (known) OOD data during training. Oftentimes the OOD samples observed during training come from a data set that is very similar to the OOD data used for evaluation. For exact details regarding the data sets and the methods used for the benchmark, we refer the reader to (Cao et al., 2020).

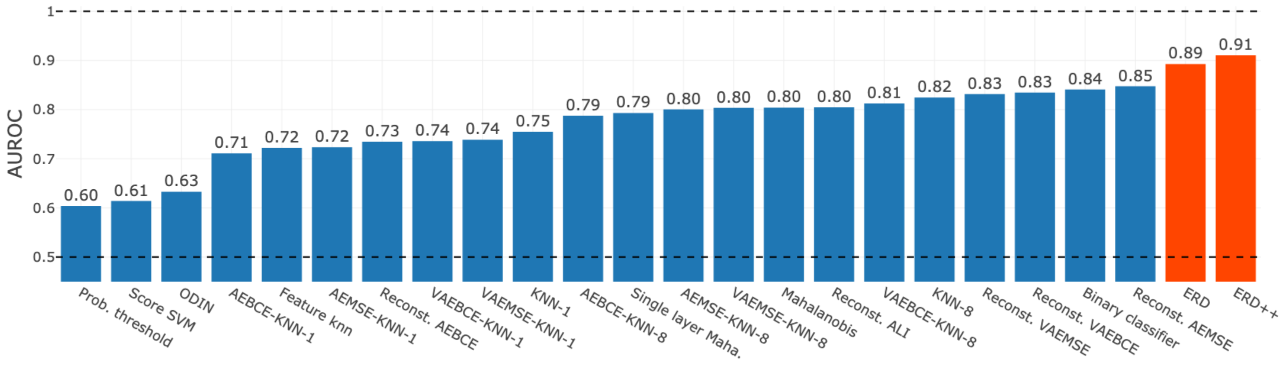

Figure 8. AUROC averaged over all scenarios in the medical OOD detection benchmark (Cao et al., 2020). The values for all the baselines are computed using code made available by the authors of (Cao et al., 2020). Notably, most of the baselines assume oracle knowledge of OOD data at training time.

In addition, in Figure 9 we present the average taken over only the novel-class settings in the medical benchmark. We observe that the performance of all methods is drastically affected, all of them performing much worse than the average presented in Figure 8. This stark decrease in AUROC and TNR@95 indicates that novelty detection is indeed a challenging task for OOD detection methods even in realistic settings. Nevertheless, our method maintains a better performance than the baselines.

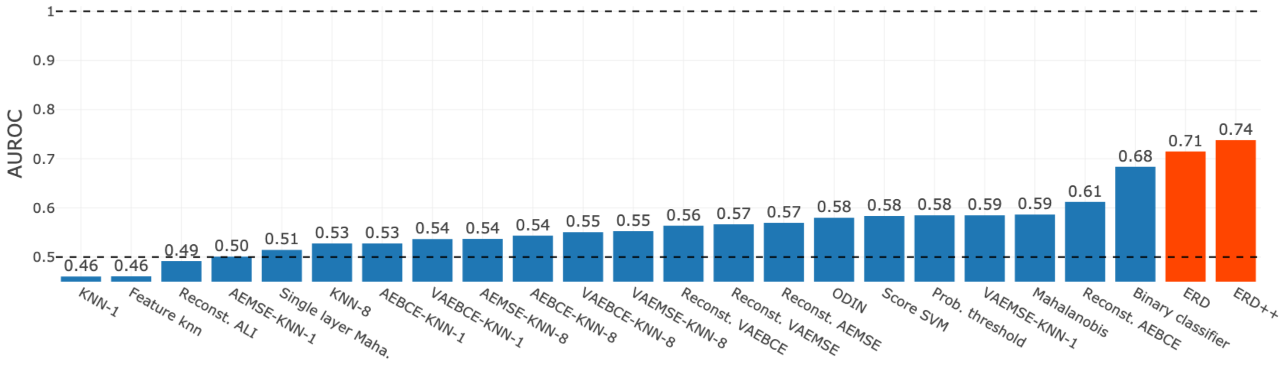

Figure 9. AUROC averaged over the novel-class scenarios in the medical OOD detection benchmark (Cao et al., 2020), i.e. only use case 3.

In Figures 10, 11, 12 we present AUROC and AUPR (Area under the Precision Recall curve) for ERD for each of the training data sets, and each of the use cases. Figure 8 presents averages over all settings that we considered, for all the baseline methods in the benchmark. Notably, ERD performs well consistently across data sets. The baselines are ordered by their average performance on all the settings (see Figure 8).

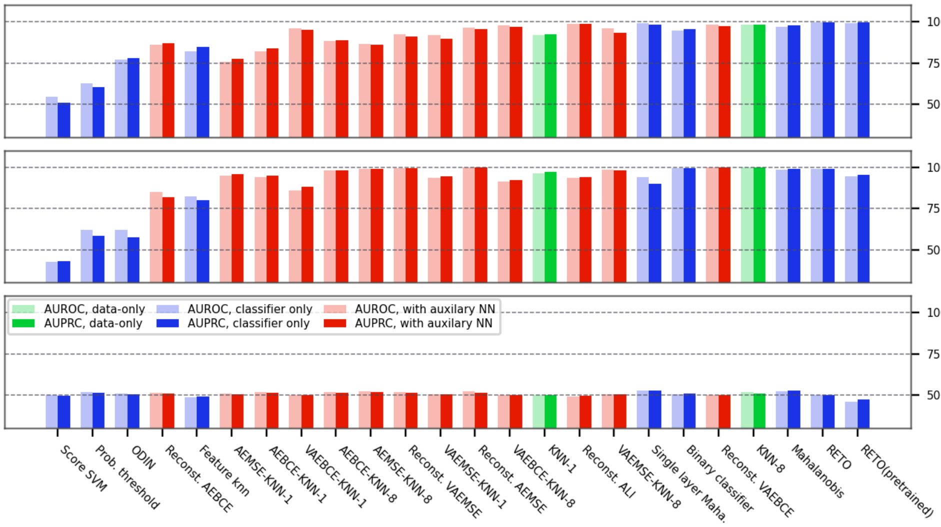

Figure 10. Comparison between ERD and the various baselines on the NIH chest X-ray data set, for use case 1 (top), use case 2 (middle) and use case 3 (bottom). Baselines ordered as in Figure 8.

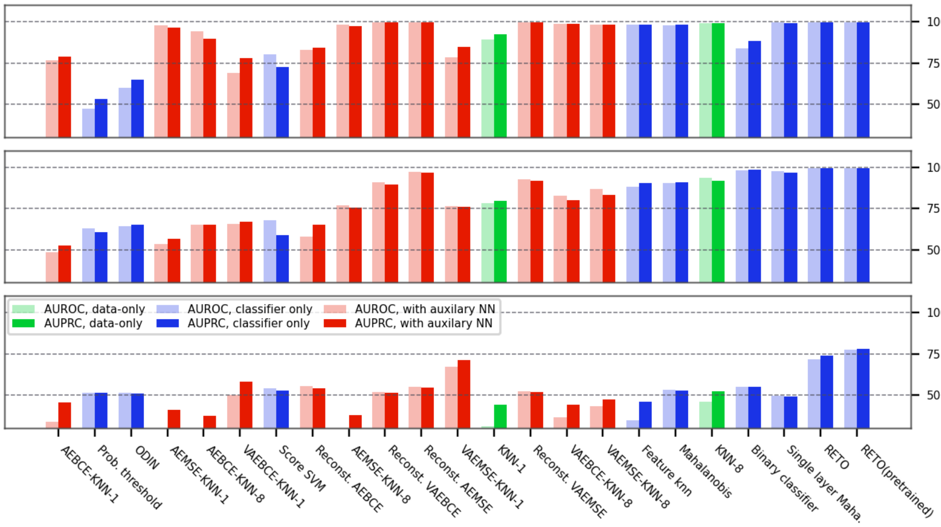

Figure 11. Comparison between ERD and the various baselines on the PC chest X-ray data set, for use case 1 (top), use case 2 (middle) and use case 3 (bottom). Baselines ordered as in Figure 8.

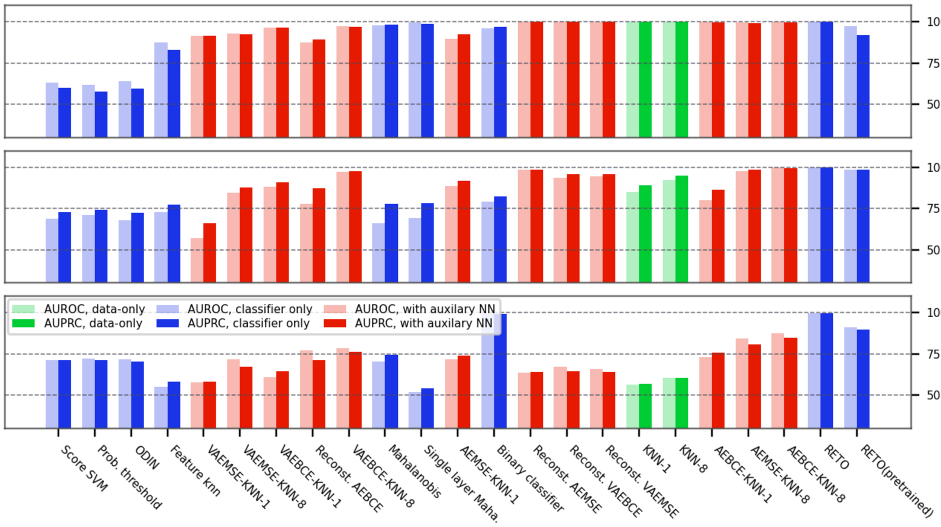

Figure 12. Comparison between ERD and the various baselines on the DRD fundus imaging data set, for use case 1 (top), use case 2 (middle) and use case 3 (bottom). Baselines ordered as in Figure 8.

For all of medical benchmarks, the unlabeled set is balanced, with an equal number of ID and OOD samples (subsampling the bigger data set, if necessary). We use the unlabeled set for evaluation.

H. Effect of learning rate and batch size

We show now that our method ERD is not too sensitive to the choice of hyperparameters. We illustrate this by varying the learning rate and the batch size, the hyperparameters that we identify as most impactful. As Figure 13 shows, many different configurations lead to similar OOD detection performance.

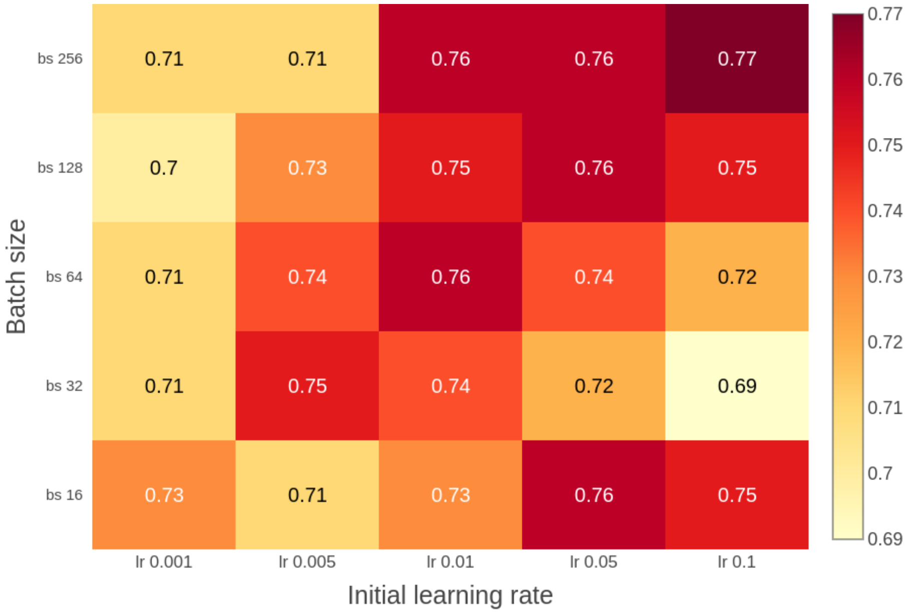

Figure 13. AUROCs obtained with an ensemble of WRN-28-10 models, as the initial learning rate and the batch size are varied. We used the hardest setting, CIFAR100:0-50 as ID, and CIFAR100:50-100 as OOD.